Photovoltaics

International Edition: DOI: 10.1002/anie.201409290
German Edition: DOI: 10.1002/ange.201409290

Biomass-Derived Carbon Quantum Dot Sensitizers for Solid-State Nanostructured Solar Cells

Joe Briscoe, Adam Marinovic, Marta Sevilla, Steve Dunn, and Magdalena Titirici**

Abstract: *New hybrid materials consisting of ZnO nanorods sensitized with three different biomass-derived carbon quantum dots (CQDs) were synthesized, characterized, and used for the first time to build solid-state nanostructured solar cells. The performance of the devices was dependent on the functional groups found on the CQDs. The highest efficiency was obtained using a layer-by-layer coating of two different types of CQDs.*

Carbon quantum dots (CQDs) have recently emerged as a new family of 0D nanocarbon materials.[1] They are spherical nanoparticles with sizes below 10 nm and exhibit excitation-wavelength-dependent photoluminescence (PL) behavior. Mechanistically, both the optical absorption and fluorescence emissions in carbon dots do not originate from a band gap, but instead are due to π-plasmon and radiative recombination of the surface-confined electrons and holes, different from those in conventional semiconductor QDs.[2–5]

The synthetic method for the production of carbon quantum dots can be divided in two main categories: top-down and bottom-up methods. Top-down methods involve "breaking" larger carbon structures into smaller pieces while the bottom-up methods rely on forming the CQDs from molecular precursors. The bottom-up method has clear advantages in terms of sustainability and compliance with green-chemistry principles, in particular when biomass precursors are used for the production of CQDs.[2,6–8]

Hydrothermal carbonization (HTC) has arisen as a powerful and sustainable technology for the synthesis of nanostructured carbon materials with a wide range of applications including renewable energy, water treatment, catalysis and gas storage.[9] During the hydrothermal carbonization of biomass or biomass precursors, first the cellulose is hydrolyzed into glucose and further dehydrated to 5-hydroxymethylfurfural (HMF) and levulinic acid. The process continues by a cascade of chemical reactions involving mainly Diels–Alder cycloadditions and ring-opening reactions.[10] During this step, nucleation occurs, forming small nucleation clusters which, upon increased reaction time, grow into micrometer scale carbon particles. Several groups have reported the use of hydrothermal carbonization of biomass to produce CQDs, which are the nucleation clusters forming prior to the growth into the final micrometer-sized carbon particle materials.[2,7,11,12]

To date, the vast majority of the applications related to CQDs are in the field of medical diagnostics and bioimaging.[13–15] Recently, CQDs have also been used for catalysis,[7] and the development of novel optoelectronic materials, such as LEDs[16,17] and solar cells, where mesoporous TiO_2 was sensitized with CQDs derived from the dehydration of γ-butyrolactone using sulfuric acid.[18] In addition, the related graphene quantum dots have been used as sensitizers in ZnO nanorod-based solar cells, but this carbon material was produced using top-down methods.[19]

Such nanostructured solar cells have the potential to be produced at significantly lower costs than traditional silicon and thin-film photovoltaics because the use of a high surface area scaffold, most commonly TiO_2 or ZnO, reduces the required absorber thickness.[20] The most common such device is the dye-sensitized solar cell, which uses TiO_2 sensitized with a ruthenium-based dye.[21] For these systems the potential for cost reduction is limited by the scarcity of this platinum-group metal. A wide range of alternative materials have been investigated to replace these dyes, including extremely thin semiconductor layers,[20] semiconductor QDs such as PbS,[22] CdSe,[23] and CdTe,[24] and alternative dyes.[25] Many of these are either costly to produce or contain toxic elements such as Pb and Cd.

Herein we propose the replacement of these expensive and unsustainable materials with biomass-derived CQDs. Three different types of CQDs with and without nitrogen functionalities were used for the first time as sensitizers for ZnO-nanorod-based solid-state nanostructured solar cells.

These CQDs were prepared by a simple one-step hydrothermal carbonization of glucose, chitin, and chitosan: three abundant and renewable precursors present in lignocellulosic biomass and most food-waste. The ZnO nanorods were synthesized using a low-temperature aqueous method (Scheme 1).

We provide a complete characterization of the nanostructured carbon materials and clearly show the importance of the different surface functionalities for the ZnO nanorod sensitization and solar-cell performance. Our approach combines the inexpensive, inorganic materials ZnO and CuSCN as electron and hole conductor with CQDs derived from biomass. The use of a solid-state hole conductor overcomes instability issues associated with liquid electrolytes and their

[*] Dr. J. Briscoe,[+] A. Marinovic,[+] Dr. S. Dunn, Dr. M. Titirici
School of Engineering and Materials Science
Queen Mary University of London
Mile End Road, E1 4NS, London (UK)
E-mail: s.c.dunn@qmul.ac.uk
m.m.titirici@qmul.ac.uk
Dr. M. Sevilla
Instituto Nacional del Carbón (CSIC)
Francisco Pintado Fe, 26
Ap. Co. 73, 33011 Oviedo (Spain)
[+] These authors contributed equally to this work.

Supporting information for this article is available on the WWW under http://dx.doi.org/10.1002/anie.201409290.

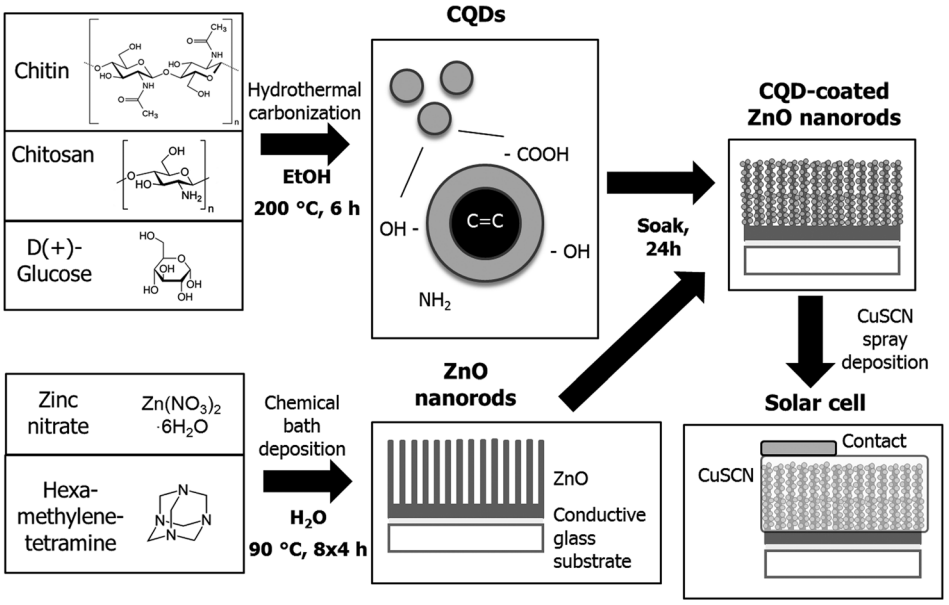

Scheme 1. Preparation of carbon quantum dot (CQD) sensitized solar cell by hydrothermal carbonization of biomass precursors, and combination with chemically grown ZnO nanorods.

potential reactions with the CQDs. CuSCN allows full infiltration of the high aspect ratio ZnO nanorods, which is not possible with organic alternatives, such as 2,2′,7,7′-tetrakis-(*N*,*N*-di-4-methoxyphenylamino)-9,9′-spirobifluorene (spiro-OMeTAD), which is also considerably more expensive. Thus, the entire solar-cell device can be produced simply and inexpensively.

The resulting CQDs were first characterized using elemental analysis, X-ray photoelectron spectroscopy (XPS), and FT-IR. As expected, the carbon content is very similar for all three CQDs at around 50% (Figure S1, Supporting Information). The chitin-derived (CT-CQDs) and chitosan-derived (CS-CQDs) CQDs contain 10.26% and 8.84% nitrogen, respectively. XPS was used to investigate the presence of different functional groups on the surface of the CQDs. The peak at 399.6 eV in the nitrogen XPS (Figure 1 a,b) demonstrates the presence of amine and/or amide groups in the CT-CQDs and CS-CQDs. The large peak at 285.5 eV in carbon-XPS (Figure 1 d) of CS-CQDs—attributable to C–N or C–C groups—and its absence in the CT-CQD spectrum (Figure 1 c) suggests the N 1s 399.6 eV peak may be predominantly amine in the case of CS-CQDs and amide for CT-CQDs. This assignment is supported by the very small contribution from H-bonded or protonated amine at 401.1 eV in N-XPS of CT-CQDs, which is much larger for CS-CQDs. FT-IR analysis (Figure 1 f and Supporting Information) confirms the retention in the CQDs of the amide and amine groups from the chitin and chitosan precursors, respectively; CT-CQDs show strong amide absorption bands at 1652 cm^{-1}, 1620 cm^{-1}, and 1570 cm^{-1}, coupled with amine N–H stretching in the region of 3200 cm^{-1}. The 3200 cm^{-1} amine band is much stronger for CS-CQDs, and coupled with N–H bending peak at 1575 cm^{-1} this again supports the dominance of amine groups in CS-CQDs. Finally, carbon XPS (Figure 1 e) and FT-IR (Figure 1 f and Supporting Information) of glucose-derived CQDs (G-CQDs) confirm the presence of -OH groups and C-O-C linkages by the XPS peak at 286.4 eV, and -OH stretching vibrations at 3600–3200 cm^{-1}. These data demonstrate that the functionalities are maintained from the original precursor into the final composition of the CQDs under these mild conversion temperatures (200 °C).

UV/Vis absorption spectra of the as prepared CQDs show a strong absorption peak at 254 nm, 268 nm, and 284 nm for chitin, chitosan, and glucose-derived CQDs, respectively (Figure S5). All the materials show a weak absorption tail extending into the visible region of the solar spectrum making them good candidates for a solar absorber material. This is in good agreement with other reports on CQDs.[2] Full details of the peaks identified in XPS and FT-IR spectra can be found in the Supporting Information.

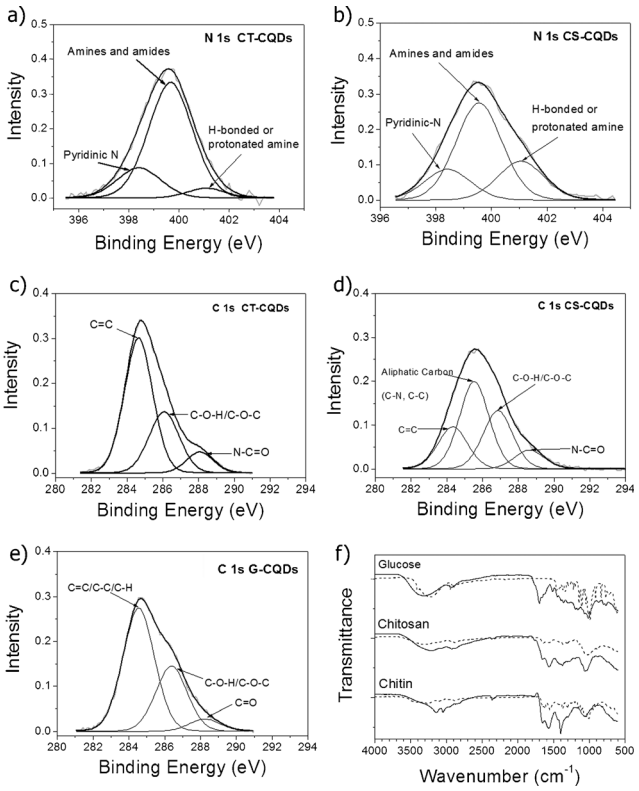

Figure 1. XPS and FT-IR spectra of CQDs. Nitrogen 1s XPS spectrum of a) CT-CQDs and b) CS-CQDs showing fit based on contributions from nitrogen species as indicated. Carbon 1s spectra of c) CT-CQDs, d) CS-CQDs, and e) G-XPS showing fits as indicated. f) FT-IR spectra of CQDs derived from all three precursors as indicated, with the initial precursor FT-IR spectra overlaid as dashed lines.

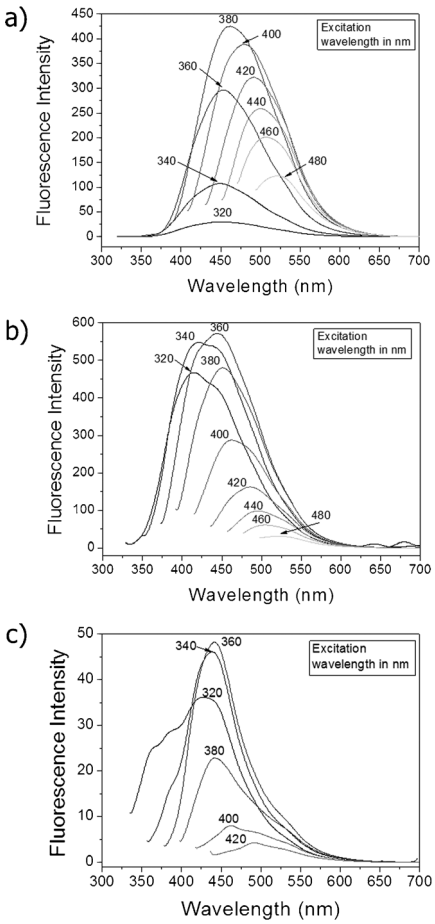

Figure 2. Fluorescence spectra of CQD samples derived from: a) chitin, b) chitosan, c) glucose.

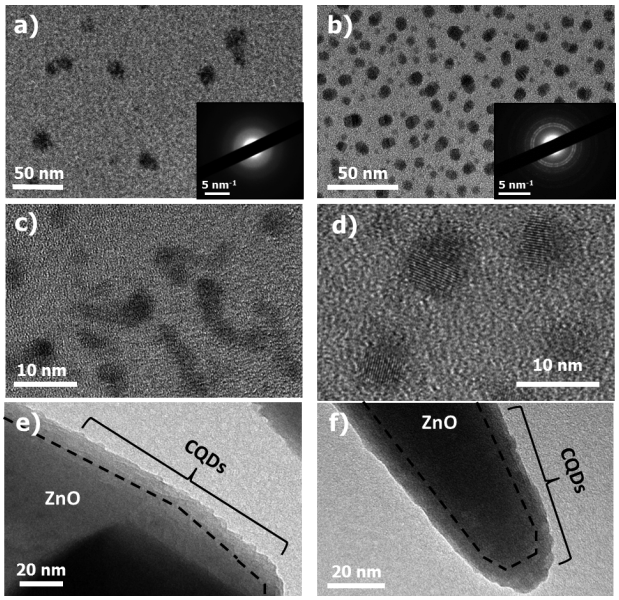

Figure 3. TEM images of CQDs derived from a) chitin, b) chitosan, c) glucose. Insets: electron diffraction. d) HRTEM of CS-CQDs. e,f) TEM images of ZnO nanorods coated with CQDs derived with a single coating of e) G-CQDs and f) 4 layers of CS + G-CQDs. Clear texturing on the otherwise smooth, crystalline ZnO surface indicates coverage by CQDs highlighted by a dashed line to show the ZnO–CQD interface.

The fluorescence spectra of the aqueous CQDs solution are given in Figure 2 and optical and fluorescence images are shown in Figure S6. The excitation-dependent emission can be clearly observed, where the emission peaks shift to higher wavelengths as the excitation wavelengths increase from 320 nm to 480 nm. Emission maxima are all centered in the visible region of the spectrum. The different functional groups present on the surface of our materials (carboxylic groups, hydroxy groups, amines, amides) in conjunction with the sp^2-hybridized carbon core are responsible for the photoluminescent properties. However, the optical properties of CQDs are to date not clearly explained in the literature and several research efforts (including our own) are currently focused on a more fundamental understanding of this phenomenon. The Supporting Information shows digital photographs of the as-obtained CQDs solutions from different precursors under daylight and under UV light. The CQDs solutions are yellowish or brown, transparent and clear under daylight and exhibit strong green luminescence under UV light (365 nm). This corresponds well with the fluorescence results (Figure 2) where all the CQDs excited at 360 nm show strong fluorescence emission in the blue/green region of the visible spectrum. The fluorescent quantum yield (QY) of the aqueous CQDs solution was calculated to be 11.6% for CT-CQDs, 13.4% for CS-QDs, and 1.4% for G-CQDs (see Experimental Section).

Figure 3a–c shows the TEM micrographs of the three different types of CQDs. The CQDs are largely monodispersed, with some potential agglomeration for G-CQDs (Figure 3c), and have spherical morphologies. Size distribution measurements show that the average diameter of the obtained CT-CQDs is (14.1 ± 2.4) nm while the CS-CQDs are (8.1 ± 0.3) nm, and the G-CQDs are much smaller with an average diameter around (2.57 ± 0.04) nm (See Figure S7). It is difficult at this stage to provide an explanation for the size difference between the various precursors. In the case of nitrogen-containing carbohydrates the CQDs presumably involve Maillard reactions between the resulting HMF and the nitrogen compounds formed during the HTC treatment[26] which explains the larger size. Glucose forms CQDs involving a single molecular species (i.e. HMF) resulting in smaller particles. Whatever the nucleation mechanism, clearly the molecular precursor has a clear influence on the CQD size under the same synthetic conditions.

The HR-TEM images of the N-containing CQDs show a graphitic crystalline structure with a repeating distance between the fringes of (0.325 ± 0.007) nm, determined using ImageJ software (Figure 3d). Electron diffraction confirms that the resulting CQDs are crystalline showing a lattice fringe of (0.318 ± 0.002) nm (see insets of Figure 3). The presence of the graphitic structure is also confirmed by the sp^2 carbon fraction observed in C 1s peak (284.6 eV, 284.3 eV, and 284.6 eV for CT-, CS-, and G-CQDs, Figure 1) as well as by the presence of signals for C=C bonds and ring vibrations in the FT-IR results (See Supporting Information for details).

After soaking in the CQD solutions for 24 h, the CQDs adhered to the ZnO nanorod surface as can be seen in the TEM image in Figure 3e, appearing as a roughening of the nominally smooth ZnO surface. Analysis of the average carbon content of the samples from wide-area SEM-EDX scans shows it to increase from around 5% for uncoated nanorods (arising from atmospheric and synthesis-related impurities) up to 10–11% for CS-CQD and G-CQD-coated nanorods, and 7% for CT-CQDs. The presence of additional carbon supports the TEM evidence that the nanorods have been coated by the CQDs, and implies that the CS- and G-CQDs coat the nanorods more densely or thickly than the CT-CQDs.

UV/Vis transmission spectra show that the transmission of the CS- and G-CQD-coated rods is decreased in the 400–550 nm range (Figure 4a), indicating they have successfully sensitized the ZnO nanorods to visible light through the visible absorption tails discussed above. The transmission of the CT-CQD-coated ZnO varies very little from uncoated ZnO, reflecting the low level of carbon detected in this sample. This situation is in good agreement with the XPS and FT-IR results which clearly show free amine groups in the case of CS-CQDs which facilitate their binding onto the ZnO surface by electrostatic interactions, which is hindered by the amide group on the CT-CQDs.

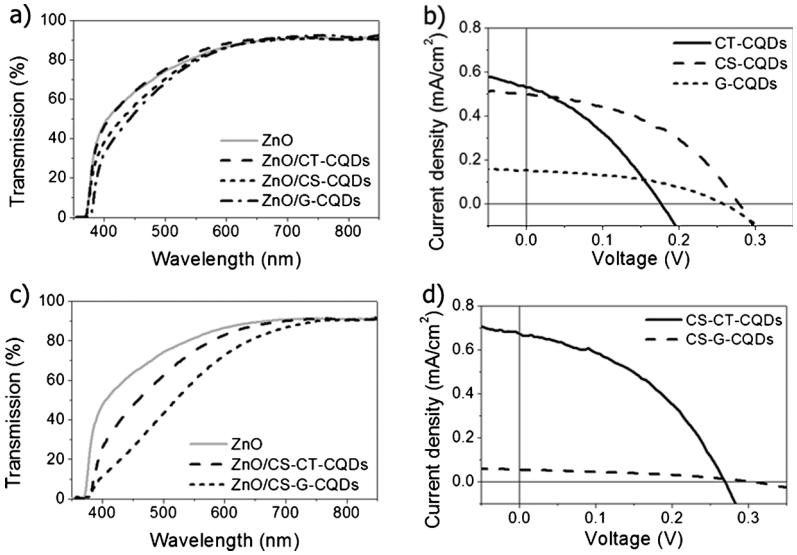

Figure 4. UV/Vis transmission for ZnO nanorods coated with CQDs as indicated (a,c) and illuminated current-voltage data of ZnO/CQD/CuSCN solar cells (b,d) using either single layer of CQDS (a,b), or 4-layer LbL coating (c,d).

The solar-cell current–voltage curves in Figure 4b and associated parameters in Table 1 show that all the CQD coatings improve the efficiency compared to the uncoated (ZnO/CuSCN) device. The CS-CQD-sensitized device has the highest efficiency owing to a combination of relatively high open-circuit voltage (V_{oc}) and short-circuit current (J_{sc}) associated with relatively low series resistance (R_s) and high shunt resistance (R_{sh}). Despite having the highest light absorption, the G-CQD-sensitized device has the lowest J_{sc} giving it a low efficiency owing to a high R_s. The CT-CQD-sensitized device also has lower efficiency, associated with a low R_{sh} and therefore low fill factor (FF) and V_{oc}. The low correlation between light absorption and J_{sc} and large variability in internal resistance suggests that the solar-cell performance is determined more by the structural nature of the coating than its light-harvesting ability; the thicker G-CQD layer enables high light absorption, but may limit collection of photogenerated carriers because of internal recombination.[27–29] Conversely the low density of CT-CQDs on the ZnO surface may not be sufficient to reduce interfacial recombination leading to a low R_{sh}. This situation demonstrates the strong dependence of the solar-cell performance on the type of CQD precursor used and the subsequent functionalization of the CQD surface. It is likely that the functionalization determines the binding of the CQD to the ZnO surface and the nature of the charge transport in the layer, influencing the solar cell performance.

Table 1: Solar-cell parameters for CQD-sensitized ZnO nanorod solar cells derived from *J–V* characteristics in Figure 4.

Sample	J_{sc} [mA cm^{-2}]	V_{oc} [mV]	FF	PCE [%]	R_s [kΩ]	R_{sh} [kΩ]
Uncoated	0.083	15	0.34	0.0004	0.27	0.30
Chitin	0.530	175	0.35	0.032	0.98	4.11
Chitosan	0.500	275	0.44	0.061	1.13	15.9
Glucose	0.153	255	0.44	0.017	3.05	40.0
Chitosan–chitin	0.674	265	0.43	0.077	0.85	9.18
Chitosan–glucose	0.054	300	0.38	0.006	14.1	66.1

The efficiency of 0.061% for the CS-CQD-sensitized device is lower than the TiO_2-based CQD solar cell mentioned above.[18] To increase light absorption while altering the composition of the coating layer, layer-by-layer (LbL) methods[22,24] were investigated by soaking ZnO nanorods in four alternating layers of either CS- and CT-CQDs or CS- and G-CQDs to utilize the opposite charges of the amine and hydroxy groups in solution. This procedure led to a clear increase in optical absorption compared to the single-CQD samples (Figure 4c), an increase of carbon content to approximately 15%, and the coatings can be seen in the TEM images (Figure 3f). Like the glucose-only devices, the increased light absorption of the CS-G-CQD device did not lead to increased efficiency: the device had extremely low J_{sc} associated with very high R_s. This supports the hypothesis that the glucose-derived CQDs lead to high levels of recombination within the CQD layer, which is exacerbated in the thicker LbL film. The combination of CS- and CT-CQDs using the LbL method produced an increased efficiency of 0.077%. This was achieved as the use of alternate layers of CQDs led to an increased loading on the ZnO surface and therefore higher light absorption, but the effect of the functional groups of the two types of CQD on the transport properties of the film were complementary, enabling a high J_{sc} without increasing R_s or reducing *FF* and V_{oc}.

Clearly the efficiency of the devices is largely limited by the light-harvesting efficiency (LHE) of the CQDs. To separate the contribution from the light harvesting, and elucidate the dependence of efficiency on the type of CQD used, the average LHE was calculated in the range 400–850 nm. For the CS + CT-CQD devices this was around 5.7%, whereas it was only 2% for the device using CS-CQDs only. Dividing PCE by LHE gives the average internal efficiency of these devices as 1.4% and 3.0%, respectively. This result demonstrates that although the CS + CT-CQD device has marginally high light absorption, it is at the expense of internal efficiency. In addition, if a greater understanding of the origins of light absorption in these materials were achieved such that CQDs with close to 100% light absorption in this range could be engineered, devices with overall PCE values over 1% could be possible.

In conclusion, we have shown that carbon quantum dots (CQDs) can be produced simply from biomass that can be sourced from waste materials: chitin, chitosan, and glucose. The as-synthesized CQDs are functionalized with the surface groups found in the source materials. These CQDs can be used to sensitize ZnO nanorods to visible light, allowing their use in solid-state nanostructured solar cells. The performance of the devices was shown to depend on the functional groups found on the CQDs. A layer combining chitosan- and chitin-derived CQDs produced devices with the highest efficiency of 0.077%. Although these CQDs and devices can be produced extremely inexpensively and simply using solution methods, the efficiencies require further improvement to provide a useful technological alternative to current devices. The light-harvesting efficiency of the devices should be improved further, potentially by coating thicker layers of CQDs without increasing the series resistance, or by increasing the visible light absorption of the CQDs themselves by size or composition control.

Experimental Section

Chitin, chitosan (medium molecular weight), and D-(+)-glucose were used as precursors to synthesize carbon quantum dots (CQDs). The precursor (0.7 g) was dissolved in ethanol (20 mL) and placed in a Teflon-lined, stainless steel autoclave, which underwent treatment at 200 °C for 6 h. The dark brown and yellow solution obtained was centrifuged at 10000 rpm for 10 min to remove the solution containing fluorescent CQDs from the solid black precipitate. The solution of CQDs was then filtered using standard syringe filters.

ZnO nanorods were grown on fluorine-doped tin oxide (FTO) substrates seeded with ZnO by spray pyrolysis of a 0.1 M zinc acetate solution in methanol at 350 °C, modified from Ref. [30]. Seeded substrates were suspended face down in an aqueous solution of 25 mM hexamethylenetetramine (HMT) and 15 mM zinc nitrate and heated for 4 h at 90 °C, which was repeated 8 times to increase the nanorod length.[23,24]

ZnO nanorods were coated with carbon quantum dots (CQDs) by soaking the substrates in the CQD solution in ethanol for 24 h before removing and rinsing with clean ethanol to remove any poorly adhered QDs. This process was repeated in subsequent solutions to produce LbL samples.

Photovoltaic devices were completed by spray-coating the CQD-coated nanorods with a 0.15 M CuSCN solution in propyl sulfide while heating at 100 °C on a hotplate until they were completely covered with a compact layer of CuSCN, as reported previously.[31] 150 nm-thick Au contacts were evaporated to form four ca. 0.2 cm^2 devices per substrate.

Transmission electron microscopy (TEM) observations were performed on a JEOL JEM-2010 electron microscope operating at 200 kV. QD size was measured from TEM images using Image-J software. Absorption spectra of CQDs were measured using PerkinElmer Lambda LS 35 UV/Vis spectrometer. The fluorescence spectra of CQDs were measured using the fluorescence spectrometer PerkinElmer LS 55, with a slit width of 10 nm both for excitation and emission. The excitation wavelength was increased from 320 nm to 480 nm in 20 nm increments. Elemental analysis data were obtained with Vario MICRO Cube elemental analyzer system. XPS measurements were carried out on a Specs spectrometer using $Mg_{K\alpha}$ (1253.6 eV) radiation from a double anode at 150 W.

The fluorescence quantum yield of the aqueous CQDs solution was calculated using quinine sulfate as a reference and following the same procedure as described by Sahu et al.[4] Five concentrations of each of the CQDs samples and quinine sulfate were prepared, all having absorbance values less than 0.1 at 340 nm. Quinine sulfate (literature quantum yield 0.54) was dissolved in 0.1 M H_2SO_4 (refractive index 1.33) while the CQDs samples were dissolved in water. By plotting the integrated fluorescence spectra (excited at 340 nm) vs. absorbency values (at 340 nm) for CQDs and quinine sulfate, the slope of the curves were calculated, and using that data the quantum yield of the CQDs was determined.

UV/Vis transmission spectra of the CQD-coated ZnO nanorods were measured using a PerkinElmer Lambda 950 spectrometer fitted with an integrating sphere. Photovoltaic device current-voltage characteristics were measured using a Keithley 2400 SMU controlled using NI Labview. Devices were tested with 100 mW cm^{-2} illumination using a Newport Oriel class ABB solar simulator with an AM 1.5 filter.

Keywords: biomass · carbon dots · hydrothermal carbonization · solar cells · sustainable chemistry

How to cite: *Angew. Chem. Int. Ed.* **2015**, *54*, 4463–4468
Angew. Chem. **2015**, *127*, 4544–4550

[1] S. N. Baker, G. A. Baker, *Angew. Chem. Int. Ed.* **2010**, *49*, 6726–6744; *Angew. Chem.* **2010**, *122*, 6876–6896.
[2] Y. H. Yang, J. H. Cui, M. T. Zheng, C. F. Hu, S. Z. Tan, Y. Xiao, Q. Yang, Y. L. Liu, *Chem. Commun.* **2012**, *48*, 380–382.
[3] P. Yu, X. M. Wen, Y. R. Toh, J. Tang, *J. Phys. Chem. C* **2012**, *116*, 25552–25557.
[4] S. Sahu, B. Behera, T. K. Maiti, S. Mohapatra, *Chem. Commun.* **2012**, *48*, 8835–8837.
[5] Q. H. Liang, W. J. Ma, Y. Shi, Z. Li, X. M. Yang, *Carbon* **2013**, *60*, 421–428.
[6] W. Li, Z. Zhang, B. Kong, S. Feng, J. Wang, L. Wang, J. Yang, F. Zhang, P. Wu, D. Zhao, *Angew. Chem. Int. Ed.* **2013**, *52*, 8151–8155; *Angew. Chem.* **2013**, *125*, 8309–8313.
[7] A. Prasannan, T. Imae, *Ind. Eng. Chem. Res.* **2013**, *52*, 15673–15678.
[8] C. Z. Zhu, J. F. Zhai, S. J. Dong, *Chem. Commun.* **2012**, *48*, 9367–9369.
[9] M.-M. Titirici, *Sustainable Carbon Materials from Hydrothermal Processes*, Wiley, Hoboken, **2013**.
[10] N. Baccile, G. Laurent, F. Babonneau, F. Fayon, M. M. Titirici, M. Antonietti, *J. Phys. Chem. C* **2009**, *113*, 9644–9654.
[11] Z. L. Wu, P. Zhang, M. X. Gao, C. F. Liu, W. Wang, F. Leng, C. Z. Huang, *J. Mater. Chem. B* **2013**, *1*, 2868–2873.
[12] Z. C. Yang, M. Wang, A. M. Yong, S. Y. Wong, X. H. Zhang, H. Tan, A. Y. Chang, X. Li, J. Wang, *Chem. Commun.* **2011**, *47*, 11615–11617.
[13] S. C. Ray, A. Saha, N. R. Jana, R. Sarkar, *J. Phys. Chem. C* **2009**, *113*, 18546–18551.

[14] S. Chandra, P. Das, S. Bag, D. Laha, P. Pramanik, *Nanoscale* **2011**, *3*, 1533 – 1540.
[15] S. Zhu, Q. Meng, L. Wang, J. Zhang, Y. Song, H. Jin, K. Zhang, H. Sun, H. Wang, B. Yang, *Angew. Chem. Int. Ed.* **2013**, *52*, 3953 – 3957; *Angew. Chem.* **2013**, *125*, 4045 – 4049.
[16] R. Sekiya, Y. Uemura, H. Murakami, T. Haino, *Angew. Chem. Int. Ed.* **2014**, *53*, 5619 – 5623; *Angew. Chem.* **2014**, *126*, 5725 – 5729.
[17] Q. L. Chen, C. F. Wang, S. Chen, *J. Mater. Sci.* **2013**, *48*, 2352 – 2357.
[18] P. Mirtchev, E. J. Henderson, N. Soheilnia, C. M. Yip, G. A. Ozin, *J. Mater. Chem.* **2012**, *22*, 1265.
[19] M. Dutta, S. Sarkar, T. Ghosh, D. Basak, *J. Phys. Chem. C* **2012**, *116*, 20127 – 20131.
[20] J. Briscoe, S. Dunn, *Mater. Sci. Technol.* **2011**, *27*, 1741 – 1756.
[21] B. O'Regan, M. Grätzel, *Nature* **1991**, *353*, 737 – 740.
[22] A. H. Ip, S. M. Thon, S. Hoogland, O. Voznyy, D. Zhitomirsky, R. Debnath, L. Levina, L. R. Rollny, G. H. Carey, A. Fischer, et al., *Nat. Nanotechnol.* **2012**, *7*, 577 – 582.
[23] K. S. Leschkies, R. Divakar, J. Basu, E. Enache-Pommer, J. E. Boercker, C. B. Carter, U. R. Kortshagen, D. J. Norris, E. S. Aydil, *Nano Lett.* **2007**, *7*, 1793 – 1798.
[24] J. Briscoe, D. E. Gallardo, S. Hatch, V. Lesnyak, N. Gaponik, S. Dunn, *J. Mater. Chem.* **2011**, *21*, 2517 – 2523.
[25] A. Hagfeldt, G. Boschloo, L. Sun, L. Kloo, H. Pettersson, *Chem. Rev.* **2010**, *110*, 6595 – 6663.
[26] N. Baccile, G. Laurent, C. Coelho, F. Babonneau, L. Zhao, M.-M. Titirici, *J. Phys. Chem. C* **2011**, *115*, 8976 – 8982.
[27] K. Keis, C. Bauer, G. Boschloo, A. Hagfeldt, K. Westermark, H. Rensmo, H. Siegbahn, *J. Photochem. Photobiol. A* **2002**, *148*, 57 – 64.
[28] V. Thavasi, V. Renugopalakrishnan, R. Jose, S. Ramakrishna, *Mater. Sci. Eng. R* **2009**, *63*, 81 – 99.
[29] H. J. Snaith, L. Schmidt-Mende, *Adv. Mater.* **2007**, *19*, 3187 – 3200.
[30] A. Bashir, P. H. Wöbkenberg, J. Smith, J. M. Ball, G. Adamopoulos, D. D. C. Bradley, T. D. Anthopoulos, *Adv. Mater.* **2009**, *21*, 2226 – 2231.
[31] S. M. Hatch, J. Briscoe, S. Dunn, *Thin Solid Films* **2013**, *531*, 404 – 407.

Received: September 19, 2014
Revised: November 28, 2014
Published online: February 20, 2015

